PROFILES OF WIND DIRECTION AND SPEED IN TURBULENT EKMAN FLOW

CEDRICK ANSORGE, HAUKE WURPS

Abstract. The profiles of wind speed and direction in turbulent Ekman flow are formulated based on asymptotic theory and data from direct numerical simulation. The profile of the stream-wise component follows the classical viscous, logarithmic and wake scaling. In the outer layer, the velocity component profiles can be described by an Ekman-spiral with adapted boundary conditions that result in a reduction of the spiral-like rotation. The span-wise component poses a conceptual challenge to the channel-flow analogy in the context of asymptotic matching; it exhibits a mixed scaling in the surface layer, but follows outer scaling for most of the outer layer.

1. Introduction

Wind veer away from its geostrophic direction is (i) due to direct frictional effects in the very vicinity of the surface and (ii) due to turbulence which exerts indirect frictional effects; these effects cause a slow-down of the mean wind reducing the Coriolis force thus turning the wind in favor of the pressure gradient force. Not only does the veering set the frame of reference for surface layer theory, it also has physical effects on large and small scales. From a large-scale perspective, the veering of wind across the planetary boundary layer determines the amount of cross-isobaric mass-flux, commonly referred to as 'Ekman pumping' (Ekman, 1905), and it is thus a key factor in the life-cycle of large-scale synoptic systems. Locally, the directional shear of the wind in the upper part of the surface layer may cause a systmatic yaw for tall wind power generation devices where blades reach into the Ekman layer, i.e. that part of the boundary layer where the wind starts to turn.

Wind veer in the planetary boundary layer is commonly characterized by the surface veering angle α defined as the angle between the negative surface shear stress τ_{sfc} and the geostrophic wind. Surface veering α and geostrophic drag $Z \equiv u_\star/G$, where $u_\star \equiv \sqrt{\nu|\tau_{\mathrm{sfc}}|}$, uniquely determine the surface drag τ_{sfc} in a turbulent Ekman flow. In any quantitative description of the surface layer, the friction velocity $u_\star$ is the dynamic scale and α defines the alignment of the frame of reference. Knowledge about $u_\star$ and α is thus a pre-requisite for any quantitative theory of the surface layer and a first attempt in theoretical quantification was undertaken by Rossby and Montgomery (1935) using integral relations in the boundary layer. Asymptotic similarity theory was later used by Tennekes (1973) and Blackadar and Tennekes (1968), and–based on his seminal direct numerical simulations (DNS) of Ekman flow–, Spalart, 1989 suggested a modification to take into account effects of low to intermediate Reynolds numbers. Later on, constants were re-evaluated with a focus on the atmospheric boundary layer based on observations Högström, 1988; Högström, 1996 and numerical modelling (Spalart et al., 2008; Spalart et al., 2009; Ansorge and Mellado, 2014; Ansorge, 2019).

Date: Draft - Version June 2, 2021.

Attempts were also undertaken to obtain profiles of the wind speed: One approach is to match the inner and outer layer at a reference height; Etling (2002) and Emeis (2018) (Sec. 21.10; Eq. 21.48) choose the Prandtl-layer height to match the wind speed profiles, which, however, requires to externally prescribe the veering α at that height. A one-dimensional profile with constant veering is given by Emeis et al. (2007, Sec. 3, Eq. 3.1-3.19).

Gryning et al. (2007) present an extension of the wind-speed profile beyond the surface layer using a neutral referece profile and a stability correction; Kelly and Gryning, 2010, based on a probabilistic representation of stratification, develop a model for the long-term mean windspeed in the atmospheric boundary layer and compare this with observation at different sites; Kelly and Troen, 2016 demonstrate the effect of such improved model for wind-energy applications. In consideration of the large scale separation in geophysical flow, the rotation of the wind in the surface layer is often assumed negligible, and above investigations merely focus on the wind speed; that means, the veering of the wind with height is not described and there is little knowledge on the profile of the span-wise velocity component and the precise shape of the hodograph in the limit of a truly neutral Ekman boundary layer.

Ekman-layer models and two-layer models of the ABL take into account rotational effects at higher altitudes, for instance when the wind speed needs to be evaluated at heights on the order of 100-200 m, a particular concern when it comes to wind-power forecasting (Optis et al., 2014). Despite rotational effects being considered, the formulation of these models for the outer layer and analysis of their performance primarily focuses on wind speed. Jiang et al. (2018) recognized that the outer part of the Ekman boundary layer receives less attention in comparison with the surface layer and commence in studying the neutral problem by Large-Eddy simulation (LES). They focus on the wind speed and find an extended logarithmic layer when considering the wind speed instead of the shear-aligned component, and they eventually demonstrate by means of an analytical model that this vertical extension of the logarithmic layer may be explained by a transfer of stress to the spanwise velocity component where it is assumed that the shear vector $\tau(z)$ and stress vectors $(\partial_z U, \partial_z V)$ are aligned.

Turbulent Ekman flow is considered here as a conceptual model of the homogeneous, stationary atmospheric boundary layer over a flat surface under neutral stratification. Universal profiles of the wind vector for turbulent Ekman flow can serve as well-described limit and reference for higher-order approaches taking into account possible effects of stratification, roughness or other physical complications encountered in the realgeophysical system. While, on first sight, the study of such a strongly idealized case appears as an academic problem, it contains the essence of surface similarity as it is used in most atmospheric models, be it conceptual or numeric ones. For instance, effects of roughness are commonly incorporated by a linear transformation of vertical scale involving the roughness parameter z_0 and for larger roughness also a displacement height (Monin and Yaglom, 1975; Jacobs and Van Boxel, 1988; Högström, 1988); effects of stability are commonly accounted for by a linearization around the neutrally stratified profile (Monin, 1970; Monin and Yaglom, 1975; Högström, 1988; Högström, 1996; Sakagami et al., 2020). Such generalized profiles may also serve as better initial condition for numerical simulation of the flow, to minimize the length of initial transient periods, or as benchmark for turbulence closures that can be tuned to reproduce the neutral limit case.

Despite the strong simplifications implied by our choice of set-up, there is no straightforward approach to solving this conceptually well-defined problem. Large-Eddy simulation not only needs to be tuned for the surface shear stress and veering angle, but it also relies on sub-grid closures that often assume alignment of the stress with gradients – a questionable pre-requisite when the wind rotates with height. Despite advances in analysis of this simplified set-up (Jiang et al., 2018) [(MORE?)], there is yet insufficient understanding for a quantitative generalization of the results to arbitrary external forcing (manifest in variation of the Reynolds number). At the same time, an increasing amount of high-quality and high-resolution data from turbulence-resolving approaches is emerging due to recent advances in high-performance computing and its application to geophysical problem sets; the geophysical range of scale separation, however, is–and it will remain so for the foreseeable future–out of reach for such simulation. Here, the routinely employed concept of Reynolds-number similarity can help: it states that certain statistics (normally those of low order) become independent of the Reynolds number when scaled appropriately [Dimotakis / da Silva / Pope referece?] . It appears that for certain statistics in Ekman flow, this regime is reached with the Reynolds numbers that became possible with the increasing capabilities of supercomputering over the past years. The robust features of mean velocity profiles across a range of Reynolds numbers are exploited in this work to develop a formulation for both the stream-wise and span-wise components of the mean velocity vector as a function of the Reynolds number.

[Numerical approach, DNS, Scale-separation, Re-similarity (Dimotakis, 2000; Silva et al., 2014; Pope, 2000; Moin and Mahesh, 1998; Mellado et al., 2018)]

2. Problem Formulation and Numerical Approach

We consider here incompressible, turbulent Ekman flow, that is, the turbulent flow over a flat rotating plate, as a physical model for the truly neutral atmospheric boundary layer (ABL). The f-plane approximation is applied such that rotation only acts on horizontal velocity components; we thus neglect rotational effects on the horizontal components of velocity and dynamical effects due to latitudinal variation of the rate of rotation.

2.1. Notation and Governing Equations.

The dimensional velocity vector of the numerical simulations is $\underline{U} = (U_1, U_2, U_3) = (U, V, W)$ over the coordinate system $Oxyz$, where an approximate alignment (plus/ minus few degrees centigrade) of the direction Ox with the surface shear stress is achieved. The coordinate Oy points away from the wall, and Oz points in the span-wise direction normal to Oxy. For analysis of the results, we use two coordinate systems that are (i) exactly aligned with the surface shear stress and labelled by an upper index α as in $\underline{U}^\alpha$ for the velocity vector, and (ii) the coordinate system aligned with the free-atmosphere geostrophic wind labelled by an upper index G as in $\underline{U}^G$. We denote by $u_\star$ the modulus surface friction velocity and let $Z_\star = 1/u_\star$ for brevity.

We consider the incompressible Navier–Stokes equations for the three velocity components on the f-plane in a framework that is governed by the physical parameters (i) geostrophic wind magnitude $G = \sqrt{G_1^2 + G_3^2}$ (where $\mathbf{G} = (G_1, 0, G_3)$ is the geostrophic wind vector), (ii) Coriolis parameter f (representing the angular rotation), and (iii) kinematic viscosity ν. These yield a Reynolds number Re as non-dimensional parameter governing the system. We use the geostrophic wind as

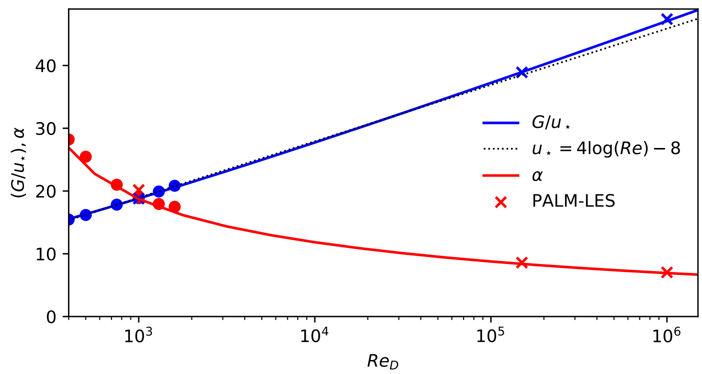

FIGURE 1. Variation of $Z_\star$ and surface veering with Reynolds number according to the theory by Spalart et al. (1989) and as estimated from DNS data

velocity and the Coriolis parameter f as time scale for the non-dimensional framework which implies the Rossby radius $\Lambda_{\mathrm{Ro}} = G/f$ as length scale, such that

$$\mathrm{Re} = \frac{G\Lambda_{\mathrm{Ro}}}{\nu}. \tag{1}$$

The non-dimensionalized set of governing equation reads as

$$\frac{\partial u_i}{\partial t} = \frac{\partial \pi}{\partial x_i} - u_j \frac{\partial u_i}{\partial x_j} + \epsilon_{i2j}(u_j - G_j) + \frac{1}{\mathrm{Re}} \frac{\partial^2 u_i}{\partial x_j^2} \tag{2a}$$

$$\frac{\partial u_j}{\partial x_j} = 0, \tag{2b}$$

where $u_i = U_i/G$ are the non-dimensional components velocity, π is non-dimensional pressure, and $g_j = G_j/G$ are non-dimensionalized components geostrophic wind (with $g_1^2 + g_3^2 = 1$ by construction).

2.2. **Numerical Simulations.** [DNS Code]

[(new and old) Simulations]

3. Towards a Universal Velocity Profile for the Turbulent Ekman Layer

Formulations for the outer layer that take into account the rotation, and thus deviation from the channel-flow analogy need to be matched to the framework of surface similarity, and it occurs that a smooth transition from the inner to the outer layer is not easily achieved. Optis et al., 2014, for instance, define an "effective geostrophic wind vector that has the same magnitude of the observed surface geostrophic wind and is rotated by the angle α [their nomenclature]" to overcome the unsteady transition when coming approaching the Ekman layer from below. While such rotation of the wind vector is *a posteriori* justified by the observational data that the model outcomes are compared to, we believe that it is the manifestation of a mismatch between the theoretical treatment of the inner and outer layer of turbulent Ekman flow.

3.1. **Drag-Law.** A drag-law for Ekman flow determines two key parameters of the flow as a function of Reynolds number alone. These are, first, the modulus of the surface friction normalized by the geostrophic wind forcing, $u_\star$ and, second, the direction of surface shear stress, α, also termed wind veering. A non-zero veering of the wind is a rather special case in comparison with most turbulent flows conisdered in an engineering context, and it confronts us with a situation where the most appropriate coordinate system for analysis (namely that aligned with the surface shear stress) is a priori unknown. We compare our DNS data against a semi-empirical drag-law based on integral consideration Spalart, 1989 and find, as demonstrated in previous work Ansorge and Mellado, 2014, excellent agreement in the range $400 < \mathbf{Re} < 1600$, representing a factor of 16 in variation of viscosity.

We also find that the solution of the transient equation involved in estimation of $u_\star$ for a given Reynolds number Re_D is approximated reasonably by the formulation

$$u_\star = 4\log(\mathbf{Re}_D)) - 8 \tag{3}$$

which quantifies the 'weak' dependence of $u_\star$ on the Reynolds number as an approximately logarithmic one, at least for problems with a scale separation on the order that is relevant to geophysical problem ($Re_D < 10^8$).

3.2. **Profile in the outer layer.** The outer layer of Ekman flow is characterized by a turning of the wind velocity and the super-geostrophic maximum that is sustained by momentum convergence at the inflection point of the velocity profile. The super-geostrophic maximum of streamwise velocity and a secondary minimum aloft the bulk-turbulent part of the boundary layer are well-described by a classic Ekman spiral with adapted boundary conditions and a shift in reference height. The textbook solution for the Ekman layer reads as [equations / figures]

3.3. **Stream-wise Velocity Component.** For the stream-wise velocity profile (that in non-rotating flows due to the geometry is always aligned with the surface shear stress), well-established theories exist for various regimes according to their distance from the wall and the relative role of viscosity, turbulence and interaction with the outer region of the flow with the logarithmic law for the mean velocity as a central anchor point.

In immediate vicinity to the surface, local turbulent mixing cannot occur for the no-slip/no-penetration boundary condition, and the mean velocity is described by a viscous profile of the form

$$(U, W)^{\alpha +} = (z^+, 0) \tag{4a}$$

where the direction of the velocity points into the exact opposite direction of the wall shear stress τ. In absence of roughness elements and for small roughness ($z_0^+ < 5$), this linear regime is known as viscous sub-layer Foken, 2002; Foken et al., 1978. In fact, this law of the wall has no degree of freedom given the drag, i.e. once $u_\star$ and α are defined. However, theoretical foundation is lacking for the exact shape of the velocity profile in the buffer layer; though crucial for turbulence production, it is commonly understood as a transition region between the linear profile at the surface and the logarithmic profile aloft. A pure blending from the linear velocity profile into the logarithmic one is, however, not reasonable as both the linear and logarithmic profile overestimate the velocity in the buffer layer. We therefore introduce a higher-order compensating term into the linear profile before blending it into the logarithmic

../plot/outer_layer.pdf

FIGURE 2

law:

$$U^{\alpha}_{\text{inner}}{}^{+} = \frac{y^+ + \gamma_4 (y^+)^4 + \gamma_6 (y^+)^6}{1 + \gamma_6 / u_{ref} (y^+)^6}, \tag{4b}$$

where the fourth- and sixth-order terms in the nominator are designed to fit the profile below $y^+ \approx 10$ and the sixth-order correction in the denominator limits the growth of u_{inner} for large y^+.

In the logarithmic region, we use the profile

$$U^{\alpha}_{\log}{}^{+} = \frac{1}{\kappa} \log y^+ + C \tag{4c}$$

with the von-Kármán constant $\kappa = 0.416$ and the boundary condition $C = 5.4605$.

3.4. **Span-wise velocity.** The background rotation and associated veering of the surface wind implies a non-zero profile for the span-wise velocity which challenges the conventional assumptions related to the so-called channel-flow analogy: While the universal profiles in vicinity of the wall implies that the profile be zero or at

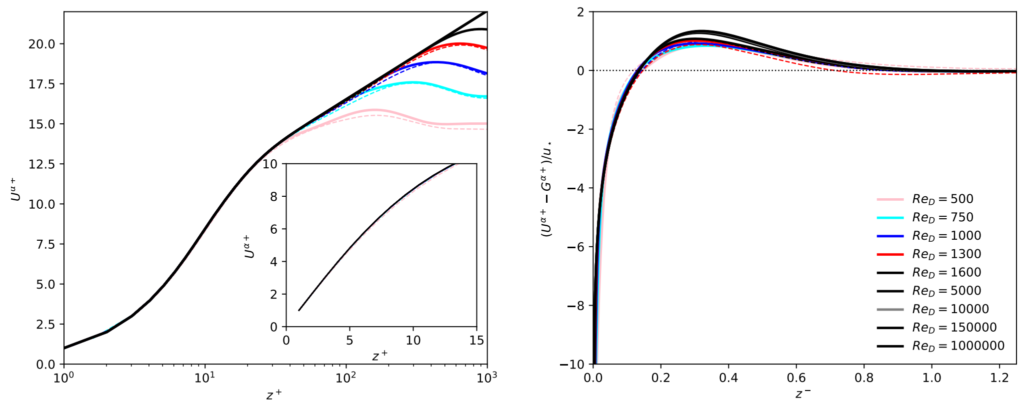

FIGURE 3. Shear-aligned profiles of velocity components $U^{\alpha+}$ in inner (left) and outer (right) units.

least small with respect to the stream-wise component, the veering requires a value of $V_{top} = U_G \sin\alpha$ in the free stream (and thus also at the top of the boundary layer if we assume that substantial velocity gradients are confined to the turbulent part of the flow). This is commonly shown in terms of velocity hodographs aligned with the outer, geostrophic flow (cf. Fig. 5) and normalized by the geostrophic wind. Thus, the drag-law already implies three important properties of these hodographs, (i) the boundary conditions at the surface, (ii) the boundary condition at the top, and (iii) the inclination of the hodograph at the origin by the surface veering:

$$\underline{U}^G(z=0) = 0, \tag{5a}$$

$$\underline{U}^G(z\mapsto\infty) = \underline{G}^G = \begin{pmatrix} 1 \\ 0 \end{pmatrix} \tag{5b}$$

$$\left.\frac{\partial V^G}{\partial U^G}\right|_{z=0} = \sin\alpha \tag{5c}$$

Outer scaling of the velocity profile further implies that the velocity deficity of the spanwise component $V^\alpha - G^\alpha$ be a universal function of the outer height z^-, i.e.

$$V^\alpha - G^\alpha = f_V^\alpha(z^-). \tag{6}$$

Interpreting the shear-aligned spanwise velocity deficit $f_V^\alpha(z^-)$ as a signature of outer rotation may lead one to conclude that this universal function is appropriate down to the surface–irrespective of the Reynolds number. This cannot be the case for the variation of $f_V^\alpha(z^-)$ across the boundary layer (i.e. between $0 < z^- < 1$) must fulfill the drag law and boundary conditions; at the same time, the weak dependence of α and $u_\star$ on Re implies this range depends on Re.
Outer Layer. In the outer region of the flow (for $z^- \mapsto 1$), $f_V(z^-)$, should govern the spanwise velocity profile which indeed is supported by our DNS data (Fig.4): The deficit is close to zero for $z^- \gtrsim 1$, and can be approximated by a logarithmic profile in the range $0.15 \lesssim z^- \lesssim 0.4$. The slope of this profile is best fit by $\kappa_V = 0.836(1 + 150/Re_D)\kappa$, where the correction term for low Reynolds number may be omitted for $Re_D \gg 1000$. Based on Fig. 4, we pick the offset as a constant fraction

(0.906) of $V_G^\alpha = Z_\star \sin\alpha$, i.e

$$V_{\log}(z^-) = \frac{1}{\kappa_V} \log\left(\frac{z^-}{0.4}\right) + 0.906 V_G^\alpha. \tag{7a}$$

The eventually converged simulations at intermediate Re_D (where the DNS could be run over several inertial periods) exhibit a super-geostrophic maximum (positiv velocity deficit) in the span-wise component. This maximum is not present or less pronounced for the simulations at higher Re where closer analysis reveals that the velocity profiles in the outer layer are still subject to a small though finite adaptation process on the inertial time scales $2\pi/f$ due to the relatively short time span for which these cases could be simulated. While there is no physical model for this wake region that leads to an analytical velocity profile formulation in the span-wise direction, an error-function transition from the outer logarithmic law to the boundary condition provides a reasonable fit:

$$V_{\text{outer}}(z^-) = (1 - w_V) V_{\log}(z^-) + w_V V_G^\alpha \tag{7b}$$

with

$$w_V = \frac{\text{erf}\left[\xi_{\text{outer}} \log(z/z_{\text{ref}})\right] + 1}{2} \tag{7c}$$

where ξ_{outer} is a transition scale that defines the width of the wake region and z_{ref} defines the height. Based on the DNS data, we choose $\xi_{\text{outer}} = 2$ and let z_{ref} such that $V_{\log}(z_{\text{ref}}) = 0.98 V_G^\alpha$. There is, however, a degree of ambiguity in the exact choice of these parameters due to the imperfect convergence of the DNS data to the statistical equilibrium.

Inner Layer. It is important to note that the logarithmic layer observed here for the spanwise velocity does not conincide with the log-region of the streamwise velocity but is rather a 'continuation' through the outer layer. This is consistent with the recent finding of a second log-region in the outer region of Ekman flow (... et al. (incl. Sullivan), JAS 2019). Below this region, the gradients in span-wise velocity are rather small and the span-wise velocity monotonically approaches its surface boundary condition $V(z=0) = 0$. While the stream-wise velocity follows a universal inner scaling that has acquired its universal, Re-independent shape for $Re_D > \mathcal{O}\left(10^3\right)$, the span-wise component that defines how the velocity vector veers when the surface is approached, does not collapse in inner units, and there is, most importantly no sign of convergence even at the highest Reynolds numbers for which simulations where carried out. Even though the simplest assumption $V = 0$ is reasonable for the lower part of the surface surface layer ($z^- < 10^{-3}$), it does not appropriately capture the profile in the rest of the surface layer:

First, $V = 0$ implies a discontinuity in the velocity profile at $z^- = 0.1$, where the outer scaling found above yields a finite value at geophysical Re, i.e. there is non-zero veering in the upper part of the surface layer–as is well-known also from field observation. Second, the layer around $z^- = 0.1$ is crucial to obtain the characteristic and well-established shape of the hodographs as the layer where V sets in marks the 'maximum' of V^- vs. U^-. This illustrates that the higher-order (in terms of the channel-flow analogy where $V = 0$) correction follows a mixed scaling when the surface is approached which has been demonstrated for higher-order terms in other types of flow (Mellado et al., 2016).

The scale for the magnitude of the span-wise velocity component is $u_\star \sin\alpha$. Based on our DNS data, we suggest that the Reynolds number scaling of this velocity-magnitude scale is captured by $Re_\tau^{-1/2}$ which is indeed known from the generalization of higher-order statistics, such as turbulent fluxes in the inner layer (Marusic et al., 2013) that also follow a mixed scaling in the inner layer. We then parameterize the spanwise velocity at 10 wall units as anchor point in the inner layer:

(8a) $$V_{10} \equiv V(z^+ = 10) = 750 \frac{u_\star \sin\alpha}{\sqrt{Re_\tau}}.$$

This leaves us with three fixed points of the velocity profile in the inner layer, namely (i) the boundary condition $V_0 = 0$, (ii) V_{10} at $z^+ = 10$, and (iii) the lower end of the logarithmic profile at $z^- = 0.1$ where the latter two are semi-empirically estimated from DNS data. In absence of well-established scaling considerations for the span-wise velocity, the choice of profile fits joining these three points is indeed arbitrary, but we can resort to the DNS data for an empirical approach and find that a square-root profile fits $V(z^+)$ in the surface layer. A linear profile for V is employed in the viscous sub-layer. Based on the physical extent of the viscous sub-layer in Ekman flow around five wall units (Foken, 2002; Ansorge, 2019), we choose $z^+ = 5$ to transition from one to the other and note that V is already very small at this height. The span-wise velocity profile in the surface layer is then estimated as

(8b) $$V(z^+)\big|_{\text{inner}} = \begin{cases} a_1 z^+ & ; \quad z^+ \leq 5 \\ b_1 + b_2\sqrt{z^+} & ; \quad 5 < z^+ < Re_\tau/10 \end{cases},$$

with b_1 and b_2 estimated such that

(8c) $$\begin{array}{rcl} V(z^+ = 10)\big|_{\text{inner}} & = & V_{10} \\ V(z^+ = Re_\tau/10)\big|_{\text{inner}} & = & V_{\text{outer}}(0.1) \end{array} \Rightarrow \begin{cases} b_2 = \dfrac{V_{\text{outer}}(0.1) - V_{10}}{\sqrt{Re_\tau/10} - \sqrt{10}} \\ b_1 = V_{10} - \sqrt{10} b_2 \end{cases}$$

We then estimate α from the matching condition at $z^+ = 5$, i.e.

(8d) $$5a = b_1 + \sqrt{5} b_2 \Rightarrow a = \frac{1}{5}\left[V_{10} + (\sqrt{5} - \sqrt{10})\left(\frac{V_{\text{outer}} - V_{10}}{\sqrt{Re_\tau/10} - \sqrt{10}}\right)\right].$$

Matching region. While the profile composed of $V_{\text{inner}}(z^+ \leq 0.1Re_\tau)$, $V_{\text{outer}}(z^- > 0.1)$ is continuous, it is not smooth at $z^- = 0.1$, i.e. at the transition from power-law ($V \propto \sqrt{z^+}$) to logarithmic scaling. To alleviate this issue, we use a second-order polynomial for transition from the inner to the outer layer in the range $z_{\text{low}} < z < z_{\text{up}}$ such that

(8e) $$V_{\text{trans}}(z^-) = V_{\text{inner}}(z^+_{\text{low}}) + \Delta V\left(a z_{arg} + b(z_{arg})^2\right)$$

with $\Delta V = V_{\text{outer}}(z^-_{\text{up}}) - V_{\text{inner}}(z^+_{\text{low}})$ and $z_{arg} = (z - z_{\text{low}})/(z_{\text{up}} - z_{\text{low}})$. It is $a + b = 1$ for $V_{\text{trans}}(z^-_{\text{up}}) = V_{\text{outer}}(z^-_{\text{up}})$, and we constrain a by

(8f) $$\left.\frac{\partial V_{\text{trans}}}{\partial z^-}\right|_{z=z_{\text{low}}} = \left.\frac{\partial V_{\text{inner}}}{\partial z^-}\right|_{z=z_{\text{low}}},$$

where we find that $z^-_{\text{low}} = 0.06$ and $z^-_{\text{up}} = 0.13$ yield satisfactory agreement with DNS data.

4. Comparison with other theories

Compare to Emeis (2002) and Gryning (2007); highlight explicit knowledge on veering-profile → directional sheer;

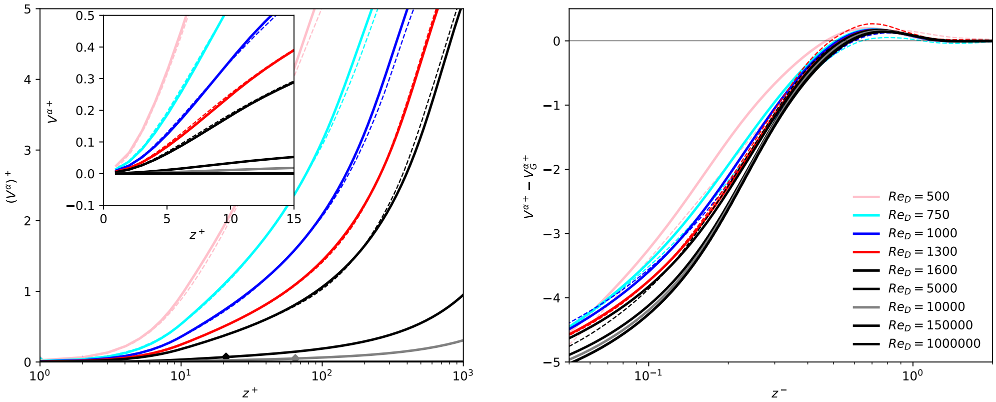

FIGURE 4. Profiles of shear-aligned span-wise velocity $(W^{\alpha})^{+}$ versus inner and outer height. Dashed lines show DNS data, thick, opaque lines are from the semi-emprical theory developed above.

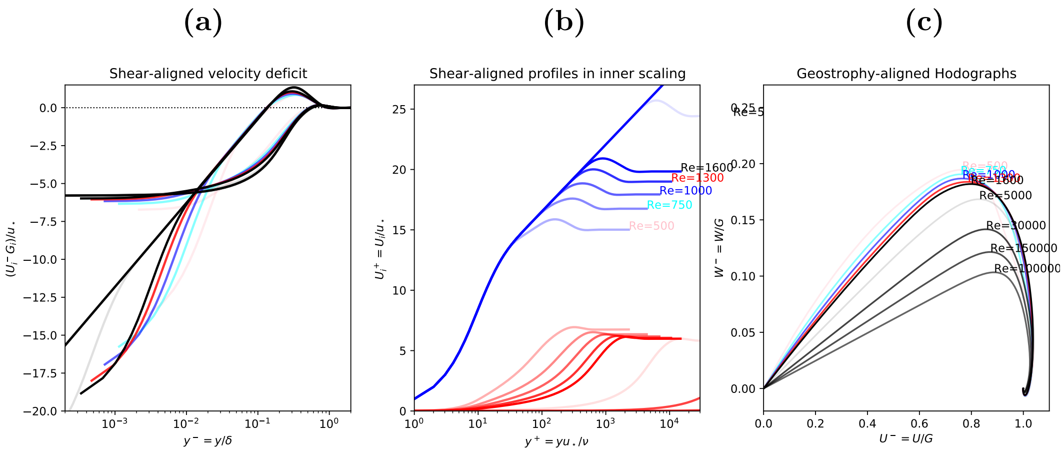

FIGURE 5. **(a)** Velocity deficity, **(b)** velocity profile in shear-aligned hodographs and **(c)** hodograph in geostrophy-aligned coordinates. Thick, solid lines show theory, dashed lines data from DNS.

Implications for **K-theory** (we now can consider that shear and stress are not necessarily perfectly aligned). $\rightarrow$ can we do something to infer a K-profile from these theoretical considerations?

5. Conclusions

Applications:

- reference-shear for neutral profile approaches(systematic!) $\rightarrow$ wind engineering!
- initial condition for LES/DNS to eliminate/minimize inertial oscillation in Benchmark simulations
-

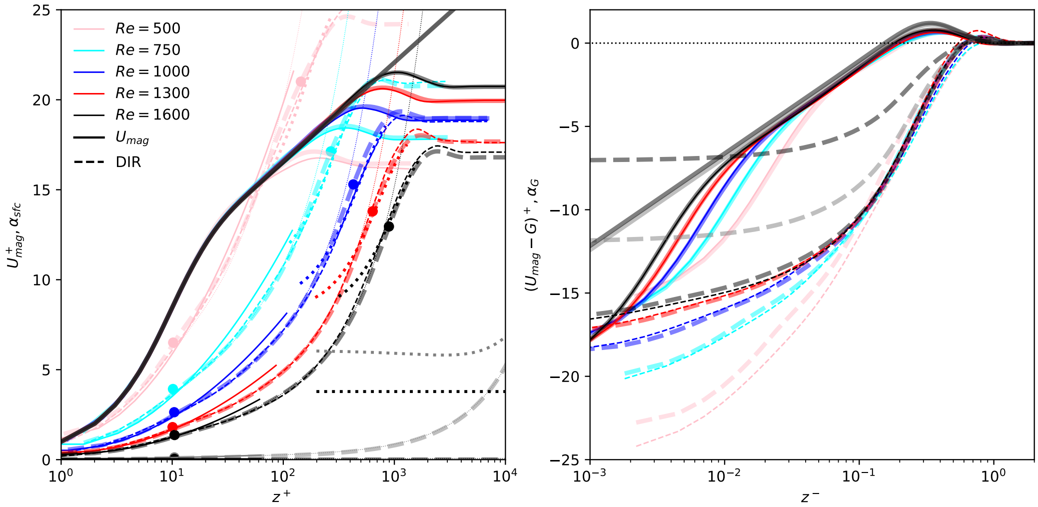

FIGURE 6. Total velocity and veering (in degrees) vs inner and outer height. Dashed lines show DNS data, thick lines are from semi-empirical theory.

APPENDIX A. LAMINAR EKMAN SOLUTION WITH CONSIDERATION OF INNER LAYER

$$\begin{pmatrix} \partial_t U \\ \partial_t W \end{pmatrix} = \begin{pmatrix} fW & + & \nu\partial_z^2 U \\ -f(U-G) & + & \nu\partial_z^2 W \end{pmatrix} \tag{9a}$$

$$\Rightarrow \partial_t(U+iW) = f(W - i(U-G)) + \nu\partial_z^2(U+iW) \tag{9b}$$

In stationary conditions, this system is solved by

$$\hat{u}(z) = U_\infty + e^{-\gamma z}\left[A\cos\gamma z + B\sin\gamma z\right] \tag{9c}$$

$$\hat{w}(z) = W_\infty + e^{-\gamma z}\left[-A\sin\gamma z + B\cos\gamma z\right] \tag{9d}$$

where the constants U_∞, W_∞ set the top boundary condition and A and B set the bottom boundary condition. The most common boundary condition for a surface Ekman layer is $A = U_\infty = G$, $B = 0$, and $W_\infty = 0$. The lower boundary condition, however, neglects the existence of the surface layer, and it appears reasonable to define $A = cG$ where $c < 1$ is a constant that icorporates the increased shear in the surface layer. Given a 'matching height' z_{match} and normalized matching height $\xi = \gamma z_{\mathrm{match}}$ in the upper part of the inner layer, we can match the Ekman profile to the inner layer by letting

$$\begin{aligned} u(z_{\mathrm{match}}) \equiv u_{\mathrm{match}} &= U_\infty + e^{-\xi}\left[A\cos\xi + B\sin\xi\right] \\ w(z_{\mathrm{match}}) \equiv w_{\mathrm{match}} &= W_\infty + e^{-\xi}\left[-A\sin\xi + B\cos\xi\right] \end{aligned} \tag{10}$$

$$\Rightarrow \begin{pmatrix} u_{\mathrm{match}} - U_\infty \\ w_{\mathrm{match}} - W_\infty \end{pmatrix} = e^{-\xi}\begin{pmatrix} A \\ B \end{pmatrix}\begin{pmatrix} \cos\xi & +\sin\xi \\ -\sin\xi & +\cos\xi \end{pmatrix} \tag{11}$$

(12)

Matching the profile at $\xi = 0$, one obtains $A = \Delta u_{\mathrm{match}}$ and $B = -\Delta w_{\mathrm{match}}$. Otherwise, it is

$$e^{\xi}\Delta u_{\mathrm{match}} = A\cos\xi + B\sin\xi \tag{13a}$$

$$e^{\xi}(\cos\xi\Delta u_{\mathrm{match}} - \sin\xi\Delta w_{\mathrm{match}}) = A(\cos^2\xi + \sin^2\xi) \tag{13b}$$

$$\Rightarrow A = e^{\xi}(\cos\xi\Delta u_{\mathrm{match}} + \sin\xi\Delta w_{\mathrm{match}}) \tag{13c}$$

$$B = \frac{e^{\xi}\Delta u_{\mathrm{match}} - A\cos\xi}{\sin\xi} \tag{13d}$$

$$= e^{\xi}\frac{\sin^2\xi\Delta u_{\mathrm{match}} + \sin\xi\cos\xi\Delta w_{\mathrm{match}}}{\sin\xi} \tag{13e}$$

$$= e^{\xi}(\sin\xi\Delta u_{\mathrm{match}} + \cos\xi\Delta w_{\mathrm{match}}) \tag{13f}$$

References

Ansorge, C. (2019). “Scale Dependence of Atmosphere–Surface Coupling Through Similarity Theory”. en. *Boundary-Layer Meteorology* 170.1, pp. 1–27. DOI: 10.1007/s10546-018-0386-y.

Ansorge, C. and Mellado, J. P. (2014). “Global Intermittency and Collapsing Turbulence in the Stratified Planetary Boundary Layer”. en. *Boundary-Layer Meteorology* 153.1, pp. 89–116. DOI: 10.1007/s10546-014-9941-3.

Blackadar, A. K. and Tennekes, H. (1968). “Asymptotic Similarity in Neutral Barotropic Planetary Boundary Layers.” *Journal of the Atmospheric Sciences* 25, pp. 1015–1020. DOI: 10.1175/1520-0469(1968)025<1015:ASINBP>2.0.CO;2.

Coleman, G. N., Ferziger, J. H. and Spalart, P. R. (1990). “A numerical study of the turbulent Ekman layer”. en. *Journal of Fluid Mechanics* 213.-1, p. 313. DOI: 10.1017/S0022112090002348.

Dimotakis, P. E. (2000). “The mixing transition in turbulent flows”. *Journal of Fluid Mechanics* 409, pp. 69–98. DOI: 10.1017/S0022112099007946.

Ekman, V. W. (1905). “On the influence of the earth’s rotation on ocean currents”. *Ark. Mat. Astron. Fys., Vol. 2 (1905), pp. 1-53* 2, pp. 1–53.

Emeis, S. (2018). *Wind Energy Meteorology.* 2nd ed. Atmospheric Physics for Wind Power Generation. Heidelberg: Springer.

Emeis, S. et al. (2007). “Wind and turbulence in the urban boundary layer analysis from acoustic remote sensing data and fit to analytical relations”. en. *Meteorologische Zeitschrift* 16.4, pp. 393–406. DOI: 10.1127/0941-2948/2007/0217.

Etling, D. (2002). *Theoretische Meteorologie.* 2nd. Eine Einführung. Berlin, Heidelberg: Springer-Verlag.

Foken, T., Kitajgorodskij, S. A. and Kuznecov, O. A. (1978). “On the dynamics of the molecular temperature boundary layer above the sea”. en. *Boundary-Layer Meteorology* 15.3, pp. 289–300. DOI: 10.1007/BF02652602.

Foken, T. (2002). “Some aspects of the viscous sublayer”. en. *Meteorologische Zeitschrift* 11.4, pp. 267–272. DOI: 10.1127/0941-2948/2002/0011-0267.

Gryning, S.-E. et al. (2007). “On the extension of the wind profile over homogeneous terrain beyond the surface boundary layer”. en. *Boundary-Layer Meteorology* 124.2, pp. 251–268. DOI: 10.1007/s10546-007-9166-9.

Högström, U. (1988). “Non-dimensional wind and temperature profiles in the atmospheric surface layer: A re-evaluation”. *Boundary-Layer Meteorology* 42, pp. 55–78. DOI: 10.1007/BF00119875.

– (1996). “Review of some basic characteristics of the atmospheric surface layer”. *Boundary-Layer Meteorology* 78.3-4, pp. 215–246. DOI: 10.1007/BF00120937.

Jacobs, A. F. and Van Boxel, J. H. (1988). “Changes of the displacement height and roughness length of maize during a growing season”. en. *Agricultural and Forest Meteorology* 42.1, pp. 53–62. DOI: 10.1016/0168-1923(88)90066-4.

Jiang, Q., Wang, S. and Sullivan, P. (2018). “Large-Eddy Simulation Study of Log Laws in a Neutral Ekman Boundary Layer”. en. *Journal of the Atmospheric Sciences* 75.6, pp. 1873–1889. DOI: 10.1175/JAS-D-17-0153.1.

Kelly, M. and Gryning, S.-E. (2010). “Long-Term Mean Wind Profiles Based on Similarity Theory”. en. *Boundary-Layer Meteorology* 136.3, pp. 377–390. DOI: 10.1007/s10546-010-9509-9.

Kelly, M. and Troen, I. (2016). “Probabilistic stability and ‘tall’ wind profiles: theory and method for use in wind resource assessment”. *Wind Energy* 19.2, pp. 227–241. DOI: 10.1002/we.1829.

Marusic, I. et al. (2013). “On the logarithmic region in wall turbulence”. en. *Journal of Fluid Mechanics* 716, R3. DOI: 10.1017/jfm.2012.511.

Mellado, J. P. et al. (2018). “DNS and LES for Simulating Stratocumulus: Better Together”. en. *Journal of Advances in Modeling Earth Systems* 10.7, pp. 1421–1438. DOI: 10.1029/2018MS001312.

Mellado, J. P., Heerwaarden, C. C. van and Garcia, J. R. (2016). “Near-Surface Effects of Free Atmosphere Stratification in Free Convection”. en. *Boundary-Layer Meteorology* 159.1, pp. 69–95. DOI: 10.1007/s10546-015-0105-x.

Moin, P. and Mahesh, K. (1998). “Direct numerical simulation: A tool in turbulence research”. *Annual Review of Fluid Mechanics* 30, pp. 539–578. DOI: 10.1146/annurev.fluid.30.1.539.

Monin, A. S. (1970). “The Atmospheric Boundary Layer”. *Annual Review of Fluid Mechanics* 2, pp. 225–250. DOI: 10.1146/annurev.fl.02.010170.001301.

Monin, A. S. and Yaglom, A. M. (1975). *Statistical Fluid Mechanics*. Ed. by J. L. Lumley. Vol. I. Mechanics of Turbulence. Dover Publications, Inc.

Optis, M., Monahan, A. and Bosveld, F. C. (2014). "Moving Beyond Monin-Obukhov Similarity Theory in Modelling Wind-Speed Profiles in the Lower Atmospheric Boundary Layer under Stable Stratification". *Boundary-Layer Meteorology* 153.3, pp. 497–514. DOI: 10.1007/s10546-014-9953-z.

Pope, S. B. (2000). *Turbulent Flows*. Cambridge University Press.

Rossby, C.-G. and Montgomery, R. B. (1935). "The layer of frictional influence in wind and ocean currents". *Papers in Physical Oceanography and Meteorology* III.3, pp. 1–101.

Sakagami, Y., Haas, R. and Passos, J. C. (2020). "Generalized Non-dimensional Wind and Temperature Gradients in the Surface Layer". en. *Boundary-Layer Meteorology* 175.3, pp. 441–451. DOI: 10.1007/s10546-020-00510-3.

Silva, C. B. da et al. (2014). "Interfacial Layers Between Regions of Different Turbulence Intensity". en. *Annual Review of Fluid Mechanics* 46.1, pp. 567–590. DOI: 10.1146/annurev-fluid-010313-141357.

Spalart, P. R. (1989). "Theoretical and numerical study of a three-dimensional turbulent boundary layer". en. *Journal of Fluid Mechanics* 205.-1, p. 319. DOI: 10.1017/S0022112089002053.

Spalart, P. R., Coleman, G. N. and Johnstone, R. (2008). "Direct numerical simulation of the Ekman layer: A step in Reynolds number, and cautious support for a log law with a shifted origin". en. *Physics of Fluids* 20.10, p. 101507. DOI: 10.1063/1.3005858.

– (2009). "Retraction: "Direct numerical simulation of the Ekman layer: A step in Reynolds number, and cautious support for a log law with a shifted origin" [Phys. Fluids 20, 101507 (2008)]". en. *Physics of Fluids* 21.10, p. 109901. DOI: 10.1063/1.3247176.

Tennekes, H. (1973). "The Logarithmic Wind Profile." *Journal of the Atmospheric Sciences* 30, pp. 234–238. DOI: 10.1175/1520-0469(1973)030<0234:TLWP>2.0.CO;2.